AGU PUBLICATIONS

Geophysical Research Letters

RESEARCH LETTER
10.1002/2017GL075086

Key Points:
- We identify all ≥1 km wide linear features outside impact craters: most are secondary crater chains and there is one set of pit chains
- Pit chains are the surface expression of subsurface fractures, and they reveal that the localized outer layer is thicker than Ceres's average
- We propose that a region of upwelling material, resulting from convection/diapirism, formed the pit chains, and we derive its characteristics

Supporting Information:
- Supporting Information S1

Correspondence to:
J. E. C. Scully,
jennifer.e.scully@jpl.nasa.gov

Citation:
Scully, J. E. C., Buczkowski, D. L., Schmedemann, N., Raymond, C. A., Castillo-Rogez, J. C., King, S. D., … Neveu, M. (2017). Evidence for the interior evolution of Ceres from geologic analysis of fractures. *Geophysical Research Letters*, *44*, 9564–9572. https://doi.org/10.1002/2017GL075086

Received 26 JUL 2017
Accepted 23 SEP 2017
Accepted article online 9 OCT 2017
Published online 14 OCT 2017

Evidence for the Interior Evolution of Ceres from Geologic Analysis of Fractures

J. E. C. Scully[1], D. L. Buczkowski[2], N. Schmedemann[3], C. A. Raymond[1], J. C. Castillo-Rogez[1], S. D. King[4], M. T. Bland[5], A. I. Ermakov[1], D. P. O'Brien[6], S. Marchi[7], A. Longobardo[8], C. T. Russell[9], R. R. Fu[10], and M. Neveu[11]

[1]Jet Propulsion Laboratory, California Institute of Technology, Pasadena, CA, USA, [2]The Johns Hopkins University Applied Physics Laboratory, Laurel, MD, USA, [3]Institute of Geological Sciences, Freie Universität Berlin, Berlin, Germany, [4]Department of Geosciences, Virginia Polytechnic Institute and State University, Blacksburg, VA, USA, [5]U.S. Geological Survey, Astrogeology Science Center, Flagstaff, AZ, USA, [6]Planetary Science Institute, Tucson, AZ, USA, [7]Southwest Research Institute, Boulder, CO, USA, [8]INAF Istituto di Astrofisica e Planetologia Spaziali (IAPS), Rome, Italy, [9]Department of Earth, Planetary, and Space Science, University of California, Los Angeles, CA, USA, [10]Lamont-Doherty Earth Observatory, Columbia University, Palisades, NY, USA, [11]School of Earth and Space Exploration, Arizona State University, Tempe, AZ, USA

Abstract Ceres is the largest asteroid belt object, and the Dawn spacecraft observed Ceres since 2015. Dawn observed two morphologically distinct linear features on Ceres's surface: secondary crater chains and pit chains. Pit chains provide unique insights into Ceres's interior evolution. We interpret pit chains called the Samhain Catenae as the surface expression of subsurface fractures. Using the pit chains' spacings, we estimate that the localized thickness of Ceres's fractured, outer layer is approximately ≥58 km, at least ~14 km greater than the global average. We hypothesize that extensional stresses, induced by a region of upwelling material arising from convection/diapirism, formed the Samhain Catenae. We derive characteristics for this upwelling material, which can be used as constraints in future interior modeling studies. For example, its predicted location coincides with Hanami Planum, a high-elevation region with a negative residual gravity anomaly, which may be surficial evidence for this proposed region of upwelling material.

1. Introduction

Prior to Dawn's arrival, dwarf planet Ceres (radius ~ 470 km) was studied via telescopic observations, which allowed for the initial determination of its dimensions and average bulk density, and provided evidence for at least partial differentiation (Drummond et al., 2014; Thomas et al., 2005). Additionally, some thermal models predicted an undifferentiated Cerean interior (Zolotov, 2009), while others predicted Ceres differentiated into two layers: a rocky interior covered by a 50–100 km thick water-ice-dominated outer layer (Castillo-Rogez & McCord, 2010; McCord & Sotin, 2005). Extensive viscous relaxation was predicted to occur within the water-ice-dominated outer layer (Bland, 2013).

A deeper understanding of Ceres's interior required Dawn's orbital observations, which refine Ceres's dimensions and bulk density (Russell et al., 2016) and also indicate partial differentiation into two layers: a rock-rich interior covered by an outer layer that is comparatively enriched in volatiles (Park et al., 2016). Dawn's images are of higher resolution than previous telescopic observations: ≥35 m/pixel (Buczkowski et al., 2016) versus 30 km/pixel (Li et al., 2006). Dawn's images reveal a heavily cratered surface, and the impact craters are less viscously relaxed (Bland et al., 2016; Hiesinger et al., 2016) than pre-Dawn predictions (Bland, 2013). Surface morphology and finite element modeling indicate that the outer layer is a mixture of <30–40% water ice/porosity and >60–70% rock/salts/clathrates (e.g., Bland et al., 2016). Dawn's ≥35 m/pixel high-resolution images also show numerous linear features on Ceres's surface, which are interpreted to derive from both impact and tectonic processes (Buczkowski et al., 2016). Here we use a subset of the linear features to gain further insights into Ceres's interior.

2. Types of Linear Features and Ejecta Distribution

We investigate Ceres's linear features by producing a global map of all ≥1 km wide visible linear features. We omit linear features that are solely within the floor of a single impact crater (see Buczkowski et al., 2017). Our global map contains 2,319 individual segments and is based on Dawn's Framing Camera and shape model

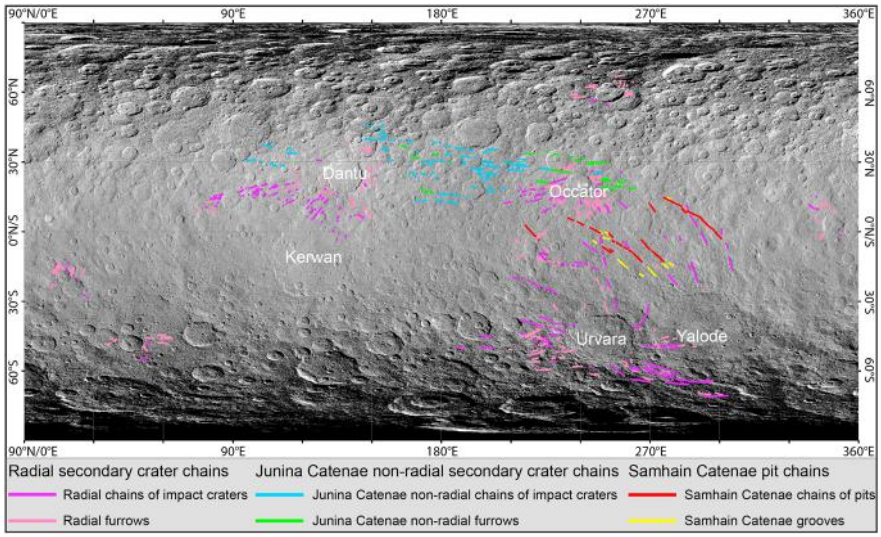

Figure 1. Global map of prominent linear features, classified by interpretation into radial secondary crater chains, Junina Catenae nonradial secondary crater chains and Samhain Catenae pit chains. Subdivisions of the linear features are discussed in Texts S2–S4 in the supporting information and in Figure 2. Impact craters discussed in the text are labeled. The basemap is the Framing Camera LAMO clear filter global mosaic (35 m/pixel) (Text S1).

data (Preusker et al., 2016; Roatsch et al., 2016) (Texts S1 and S2 in the supporting information) (Figures 1, S1, and S2). Using this global map, we identify two types of linear features: secondary crater chains and pit chains. While we use the pit chains to gain insights into Ceres's interior evolution, it is also necessary to study the secondary crater chains, to ensure that one type is not misidentified as the other. We distinguish between the secondary crater chains and pit chains using the following morphologic characteristics. Secondary craters have more clearly defined rims and more regular shapes in comparison to the pits, which have more poorly defined rims and more irregular shapes. The chains of secondary craters are often, though not always, located in a radial pattern around a source impact crater, while the chains of pits are not radial to an impact crater. The aforementioned characteristics are consistent with the formation of (i) the secondary crater chains by the impact and scour of material ejected during the formation of a source impact crater and (ii) the pit chains forming by drainage of material into a subsurface void, which is analogous to pit chains on other bodies (e.g., Wyrick et al., 2004) (Texts S3 and S4) (Figures 2 and S3). The secondary crater chains and pit chains also display different behaviors in color and spectral data (De Sanctis et al., 2015), which is similar to other bodies (Longobardo et al., 2015) (Text S5).

The most common type of linear feature segments in our map is radial secondary crater chains, which surround 13 source impact craters (Figure 1). Those around Occator, Dantu, and Urvara craters are the most prominent (Figures 1, S4, and S5). However, one group of secondary crater chains, named the Junina Catenae, is not radial to a source impact crater. "Catenae" is a term used for a chain of craters and is not associated with a specific interpretation. Thus, we use "catenae" for both chains of impact craters and chains of pit craters. The Junina Catenae are located from ~12 to 46°N and from ~95 to 265°E, are oriented ~WNW-ESE, and consist of ~11 secondary crater chains that fan out to the west (Figures 1 and S6). We find that the Junina Catenae's cumulative length is 5,400 km, their average length is 491 km, their maximum/minimum widths are 4 km/1 km, their average depth is 230 m, and their average spacing is 22 km. The Junina Catenae are crosscut by, and thus older than, Occator and Dantu craters and their associated radial secondary crater chains (Figures 1, 3, and S6).

An ejecta distribution model explains how material ejected from Urvara crater, in the southern hemisphere, formed the Junina Catenae in the northern hemisphere (Schmedemann et al., 2017) (Text S6). This model predicts that because of Ceres's low gravity (0.27 m/s^2), material ejected at ~45° and at high velocities from Urvara (~390–520 m/s) will travel above Ceres's surface for a relatively long time (~6–8 h). In comparison to bodies like the Earth, Ceres's rotation period is short (~9 h) and it is small (radius ~ 470 km) (Russell et al., 2016). Thus, by the time this material impacts the surface to form the

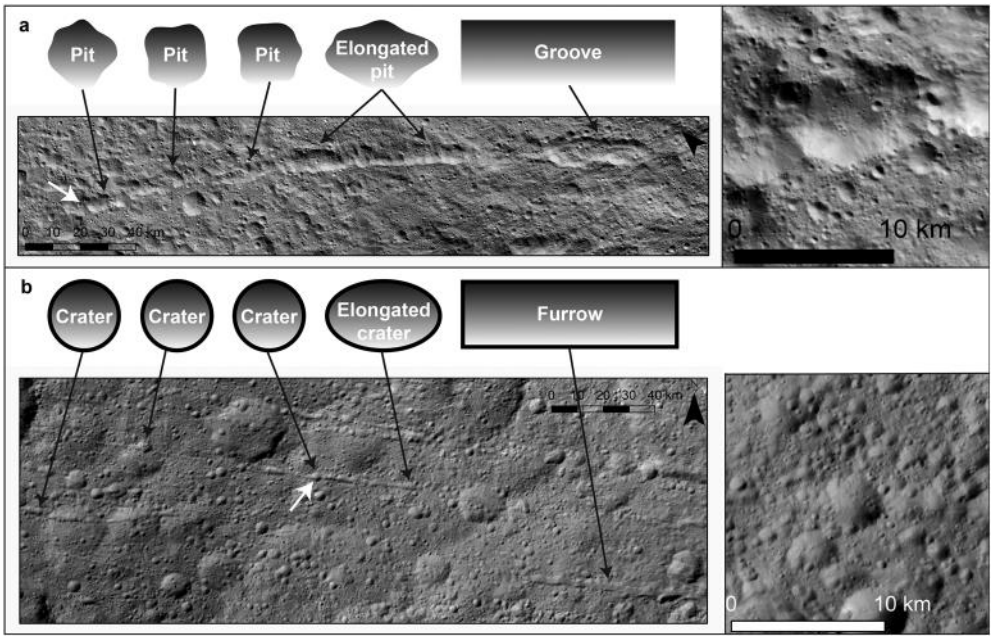

Figure 2. Schematic illustrations and examples of (a) pit chains and (b) secondary crater chains. Pit chains are made up of grooves (elongated pits) and chains of pits, which have more poorly defined rims and more irregular shapes than secondary craters (Texts S2 and S4). (b) Secondary crater chains are made up of furrows (elongated impact craters) and chains of impact craters, which have more clearly defined rims and more regular shapes than pits (Texts S2 and S3). White arrows indicate the locations of the detailed images (right).

Junina Catenae, the surface underneath it has rotated significantly, resulting in the material being located far from Urvara in a nonradial pattern. The model predictions of the location, orientation, and fan pattern of this high-velocity material are consistent with our mapping of the Junina Catenae (Figure 4). A minority of the Junina Catenae may have been formed by the impact of material from Yalode crater, which is adjacent to, and older than, Urvara (Text S7). Also consistent with our mapping, the model predicts that material ejected at lower velocities from Urvara will form radial secondary crater chains (Text S7; Figure S4). We map additional unnamed groups of secondary crater chains, also not oriented radially around a source impact crater, which we propose formed by a similar process as the Junina Catenae (Figure S2). However, ejecta distribution modeling has not yet been performed to identify the source craters of the unnamed groups.

3. Samhain Catenae Fractures and Thickness of Ceres's Outer Layer

Another set of linear features, called the Samhain Catenae, are also not radial to a source impact crater (Figures 1 and 5). The Samhain Catenae are oriented ~NW-SE between Occator and Urvara/Yalode craters. Unlike the Junina Catenae, we and Buczkowski et al. (2016) interpret that the Samhain Catenae are not secondary crater chains that originate from Urvara and/or Yalode, because the Samhain Catenae display the aforementioned morphological characteristics, and additional characteristics, that are typical of pit chains (Text S4 and Figure 2). Additionally, the Samhain Catenae are crosscut by Urvara's and Yalode's secondary crater chains, indicating that the Samhain Catenae formed first (Figures 3, 5).

The Samhain Catenae consist of approximately six pit chains, some of which are made of multiple segments. The pit chains have a cumulative length of 1,211 km, an average length of 202 km, a maximum/minimum width of 11 km/5 km, and an average depth of 1.1 km (Figure 5). The Samhain Catenae are the only set of ≥1 km wide pit chains we identify on Ceres. Consistent with analogous pit chains on other bodies (Figure S3) (Buczkowski et al., 2008; Ferrill et al., 2011; Martin et al., 2017; Scully et al., 2014; Wyrick et al., 2004), we interpret that the Samhain Catenae pit chains are the surface expression of subsurface voids at depth. Surficial material drains into the subsurface voids and forms a funnel-like shape that appears as a pit at the

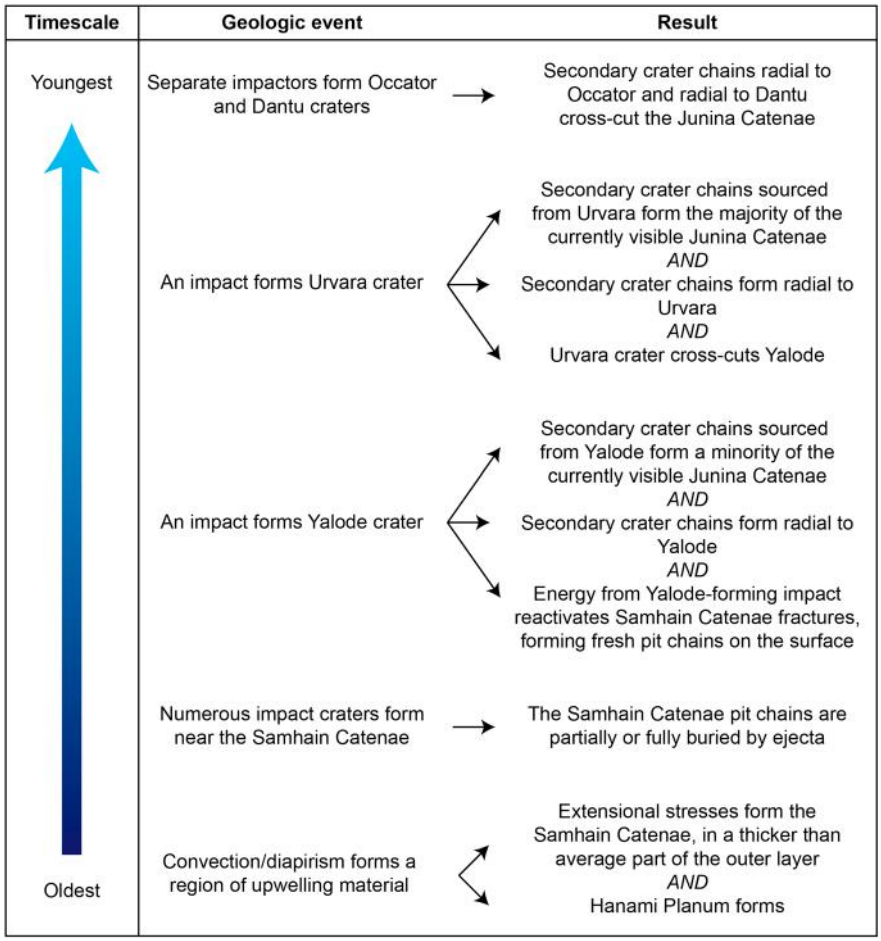

Figure 3. Timeline showing key events proposed in this work, from oldest to youngest. The details are discussed in the text.

surface. The draining surficial material is likely impact-generated debris, because Ceres is a heavily cratered body with many ejecta deposits (Buczkowski et al., 2016; Hiesinger et al., 2016). We interpret that extension fractures form the subsurface voids (Text S4).

The spacing of tectonic features is often used to estimate the thicknesses of the layers in which they occur (e.g., Bland & McKinnon, 2015; Gioia et al., 2007; Yin et al., 2016). To estimate the localized thickness of Ceres's outer layer, we use a numerically and experimentally derived ratio of extension fracture spacing to fractured layer thickness, ~0.8–1.2 (Bai & Pollard, 2000). For this ratio to apply, the fractures must cut through the entire outer layer and the region must be saturated with fractures (i.e., the region contains the maximum possible number of fractures). The Samhain Catenae fractures, as indicated by the surficial pit chains, are likely near to saturation because their spacing is relatively regular: pit chains #1–2 are ~135 km apart, #2–3 are ~48 km apart, #3–4 are ~51 km apart, #4–5 are ~104 km apart, and #5–6 are ~104 km apart (Figure 5). It is possible that additional fractures exist in the subsurface, which, if located centrally between #1–2, #4–5, and #5–6, would result in a regular fracture spacing of ~50 km. Pit chains signifying such additional subsurface fractures could have been concealed or erased from the surface by superposing impact craters and their ejecta, such as Lociyo and Kirnis (Figure 5). Despite the possibility of additional fractures at depth, we only use the spacings of the six observed pit chains in our calculations. Using the mean and standard deviation of the six pit chains' spacings, and the fracture spacing to fractured layer thickness ratio (~0.8–1.2), we estimate that the thickness of Ceres's fractured, outer layer in the localized region around the Samhain Catenae is ~58–134 km.

Ceres's average global outer layer thickness has been derived from interior models based on Dawn's gravity observations: $41.0^{+3.2}_{-4.7}$ km (Ermakov et al., 2017; Fu et al., 2017) and 43–50 km (Mitri et al., 2017). In

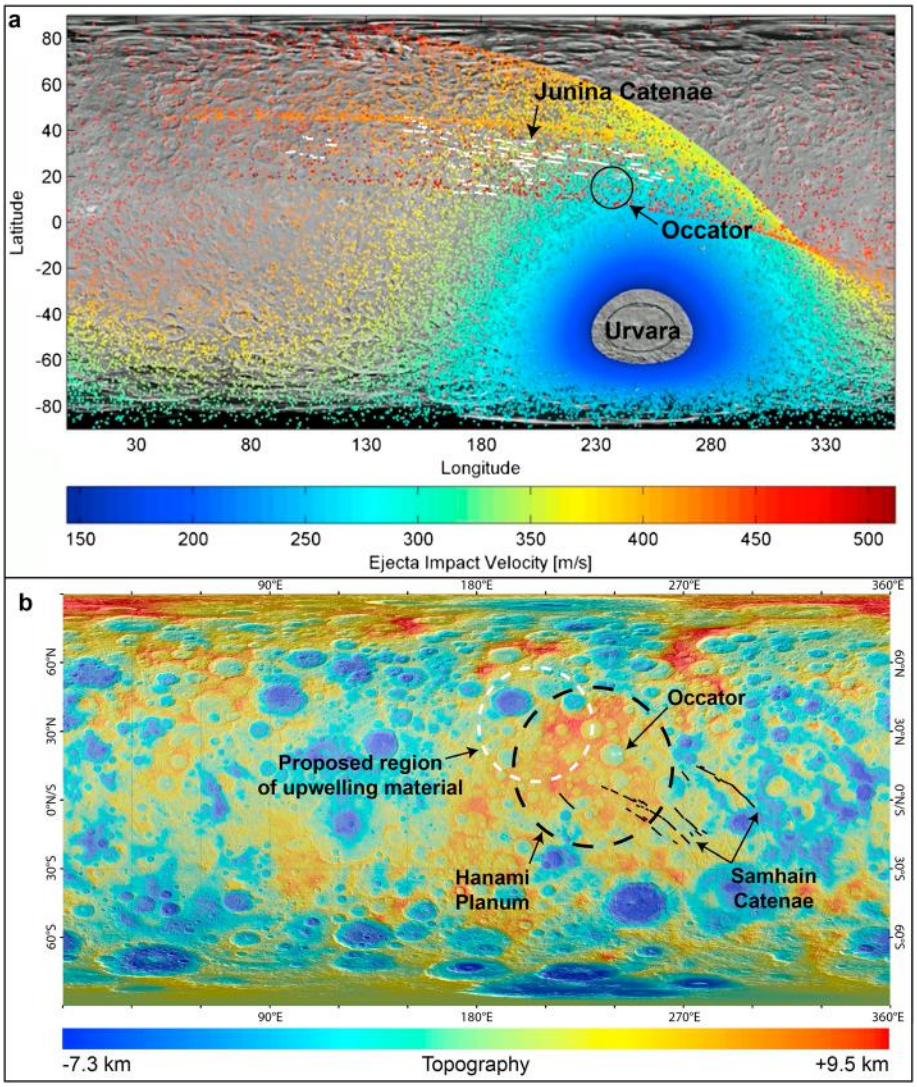

Figure 4. Formation of the Junina Catenae and Samhain Catenae. (a) Comparison between the predicted distribution of high-velocity material ejected from Urvara (red-orange dots) (Schmedemann et al., 2017) and our Junina Catenae mapping (white lines). (b) Locations of the Samhain Catenae (black solid lines), Hanami Planum (black dashed circle), and the proposed region of upwelling material (white dashed circle). The basemap is the shape model overlain onto the Framing Camera LAMO clear filter global mosaic (Text S1).

contrast, our outer layer thickness estimate only applies to the vicinity of the Samhain Catenae. Thus, our results suggest that Ceres's outer layer in this region is thicker than the global average. This is consistent with Ermakov et al. (2017), who suggest that the outer layer is thickest in a region that the Samhain Catenae are located on and adjacent to, called Hanami Planum (Figure 4). Ermakov et al. (2017) estimate that the outer layer is ~55 km thick at Hanami Planum, which is comparable to our lower estimate of the outer layer thickness (~58 km). A regional outer layer thickness of ~58 km is consistent with our aforementioned suggestion that additional fractures, whose associated pit chains have been buried or erased, result in the Samhain Catenae being spaced regularly at ~50 km. Thus, we interpret that our lower estimate, ~58 km, is most representative of Ceres's outer layer thickness in the vicinity of the Samhain Catenae. The gravity-derived outer layer thickness estimates reflect density differences between the outer layer and the underlying rock-rich interior, while our fracture-derived estimate reflects a rheology/strength difference. Therefore, the consistency between the gravity-derived and fracture-derived estimates suggest that the density and rheology/strength boundaries between the outer layer and underlying rock-rich interior occur at approximately the same depth in this region.

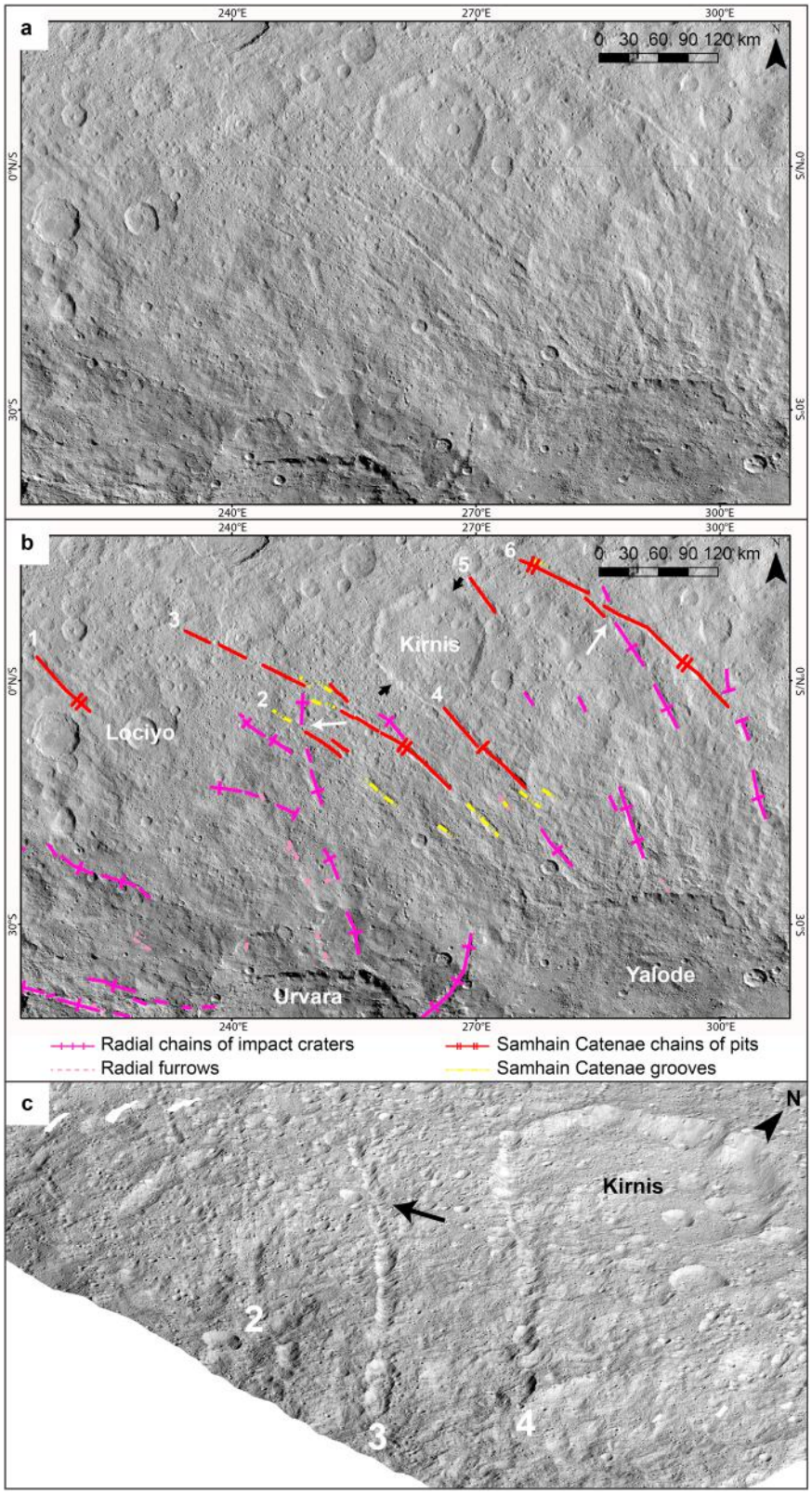

Figure 5. Samhain Catenae pit chains in (a) unmapped, (b) mapped, and (c) perspective views. In Figure 5b white arrows show example locations where Urvara/Yalode radial secondary crater chains crosscut the Samhain Catenae pit chains, which are labeled at their northwestern tips. Black arrows indicate the polygonal crater Kirnis's straight rims, which align with the Samhain Catenae. Kirnis's southern straight rim merges with Samhain Catenae #4. The basemap is the Framing Camera LAMO clear filter global mosaic (Text S1). Figure 5c shows Samhain Catenae #2–4 and an example en echelon pattern (black arrow) (Text S4).

4. Reactivation and Formation of the Samhain Catenae

Crosscutting relationships indicate that the Samhain Catenae formed first, followed by Yalode, and then Urvara craters (Figures 3 and 5). It is likely that after the Samhain Catenae's formation, events such as the deposition of impact ejecta would have partially or fully erased the initial Samhain Catenae pit chains. However, we suggest that the Samhain Catenae fractures were reactivated by the Yalode-forming impact, because the Samhain Catenae pit chains closer to Yalode are deeper than the farther pit chains (Figure S7). Reactivating the fractures would result in new surficial material draining into the fractures, forming fresh pit chains on the surface that are visible as the Samhain Catenae today. The later formation of the nearby Urvara crater, which is similar in size (170 km diameter) to Yalode (260 km diameter), could also have reactivated parts of the Samhain Catenae. In the following subsections, we investigate three hypotheses for the formation of the Samhain Catenae, which would have occurred prior to their reactivation.

4.1. Samhain Catenae Formed by a Basin-Forming Impact

The pole positions of planes defined by the Samhain Catenae fractures are located within a putative relict impact basin, suggesting that the Samhain Catenae were formed by stresses induced by the basin-forming impact (Marchi et al., 2016). However, the existence of the impact basin is unconfirmed. Also, the poles are not located at the center of the impact basin, which would provide stronger evidence for impact-induced stresses forming the fractures, as occurred on Vesta (Buczkowski et al., 2012). Consequently, in agreement with Buczkowski et al. (2016), this is not our favored formation mechanism of the Samhain Catenae.

4.2. Samhain Catenae Formed by Freezing of a Global Subsurface Ocean

Dawn data indicate that Ceres's outer layer is mixture of water ice, rock, salts, and/or clathrates (Bland et al., 2016; Fu et al., 2017; Hiesinger et al., 2016), and this mixture's tensile strength has not been measured. However, the tensile strength of water ice increases from ~0.01–1 MPa to ~2–22 MPa when mixed with silicate particles (Lange & Ahrens, 1983; Petrovic, 2003). Thus, we infer that without preexisting weaknesses such as fractures, the tensile strength of a water ice-rock-salt-clathrate mix is approximately $\geq$10 MPa.

Freezing a subsurface ocean would add ice to an overlying outer layer, thickening and inducing tensile stresses in the outer layer (Manga & Wang, 2007; Nimmo, 2004; O'Brien et al., 2015). To fracture an outer layer on Ceres with a tensile strength of $\geq$10 MPa, thickening of $\geq$10 km would be required (O'Brien et al., 2015), which could have occurred during freezing of a global subsurface ocean within a few 100 Myr after Ceres's formation (Castillo-Rogez et al., 2016). If the Samhain Catenae fractures formed via this process, we would expect to observe globally distributed fractures, as on icy satellites (e.g., Manga & Wang, 2007; Nimmo, 2004). If it is possible for Yalode, and perhaps Urvara, to reactivate fractures, as discussed earlier, then it is also likely that impact craters comparable in size to Yalode and Urvara, such as the 280 km diameter Kerwan crater (Figure 1), could also have reactivated fractures. However, the Samhain Catenae are the only $\geq$1 km wide pit chains we observe on Ceres's surface. Thus, because there were opportunities for a globally distributed fracture set to be reactivated, and hence visible across Ceres today, we interpret that globally distributed fractures are not present. Therefore, this is also not our favored formation mechanism of the Samhain Catenae.

4.3. Samhain Catenae Formed by a Region of Upwelling Material

Multiple interior evolution models predict convection approximately within Ceres's first billion years (King et al., 2016; Neveu & Desch, 2015; Travis & Feldman, 2016). Some models predict that convection continued after Ceres's first billion years, initially in the liquid state and perhaps later in the solid state (Neveu & Desch, 2015; Travis & Feldman, 2016). Additionally, upwelling of salt diapirs is proposed to occur in the geologically recent past (Buczkowski et al., 2016). Thus, we hypothesize that a region of upwelling material derived from one of these instances of convection or diapirism induced extensional stresses within a particular portion of Ceres's outer layer, to form the Samhain Catenae. Further modeling studies are needed to evaluate this hypothesis, and our analysis of the Samhain Catenae provides predictions about the proposed region of upwelling material's characteristics, which can be used as constraints by future interior modeling studies.

5. Characteristics of the Proposed Region of Upwelling Material

To form the Samhain Catenae, the proposed region of upwelling material would have the following characteristics. The proposed upwelling would have occurred before the formation of Urvara and Yalode because

we find that the Samhain Catenae are older than both. The upwelling material would induce extensional stresses greater than our previously approximated value of the outer layer's tensile strength (≥10 MPa). The extensional stresses would be approximately perpendicular to the Samhain Catenae's current orientation.

The patterns of terrestrial dike swarms are indicative of the location of the mantle plume that formed them (Ernst & Buchan, 2001) (Figure S8). Here we approximate the location of the proposed region of upwelling material by using the patterns of dikes formed by terrestrial mantle plumes as analogs to the pattern of the Samhain Catenae. This comparison is possible because both dikes and fractures are formed by tensile stresses/extension, and thus, a dike is essentially a fracture that is infilled with material. The Samhain Catenae are most consistent with the linear pattern categorized by Ernst and Buchan (2001), because (a) they are approximately parallel to one another, (b) have a higher density in their northern region, which is closer to the location of the proposed region of upwelling material, and (c) their average width increases with distance from the location of the proposed region of upwelling material (Figures S7 and S8). The average width may have also been affected by reactivation from Yalode and possible Urvara. The Samhain Catenae's linear pattern is consistent with the proposed region of upwelling material being located adjacent to the northwestern end of the Samhain Catenae, at ~36°N, ~207°E (Figure 4).

6. Conclusions

Our detailed analysis of Ceres's linear features finds that the Samhain Catenae are the only ≥1 km wide pit chains on Ceres's surface. There are also secondary crater chains formed by material ejected from nearby and distant impact craters. The Samhain Catenae's spacing indicates that Ceres's outer layer in their vicinity is approximately ≥58 km thick, which is at least ~14 km thicker than the global average. This localized outer layer thickness is consistent with gravity-derived interior model estimations (Ermakov et al., 2017) and thus provides independent confirmation for this model. Additionally, we hypothesize that a region of upwelling material, derived from convection or diapirism, formed the Samhain Catenae. We find the characteristics of this proposed region of upwelling material, which can be used as constraints in future modeling of Ceres's interior evolution. For example, we find that its approximate location broadly coincides with Hanami Planum, a topographically high region with a negative residual gravity anomaly. A subsurface buoyancy-driven anomaly combined with a high-rigidity/thick outer layer is one possible explanation for Hanami Planum (Ermakov et al., 2017). Consequently, Hanami Planum may be evidence for our proposed region of upwelling material, and the Samhain Catenae may represent surficial evidence for past interior activity.

Acknowledgments

Part of the research was carried out at the Jet Propulsion Laboratory (JPL), California Institute of Technology, under a contract with the National Aeronautics and Space Administration. We thank the Dawn Flight Team at JPL for the development, cruise, orbital insertion, and operations of the Dawn spacecraft at Ceres. We thank the instrument teams at the Max Planck Institute, German Aerospace Center (DLR), Italian National Institute for Astrophysics (INAF), and Planetary Science Institute (PSI) for the acquisition and processing of Dawn data. We thank both of the reviewers for their helpful comments. The Framing Camera data and shape model upon which we base our mapping are available on the PDS Small Bodies Node website at http://sbn.pds.nasa.gov/data_sb/missions/dawn.

References

Bai, T., & Pollard, D. D. (2000). Fracture spacing in layered rocks: A new explanation based on the stress transition. *Journal of Structural Geology*, *22*, 43–57.

Bland, M. T. (2013). Predicted crater morphologies on Ceres: Probing internal structure and evolution. *Icarus*, *226*, 510–521.

Bland, M. T., & McKinnon, W. B. (2015). Forming Ganymede's grooves at smaller strain: Toward a self-consistent local and global strain history for Ganymede. *Icarus*, *245*, 247–262.

Bland, M. T., Raymond, C. A., Schenk, P. M., Fu, R. R., Kneisl, T., Pasckert, J. H., … Russell, C. T. (2016). Composition and structure of the shallow subsurface of Ceres revealed by crater morphology. *Nature Geoscience*, *9*, 538–542.

Buczkowski, D. L., Barnouin-Jha, O. S., & Prockter, L. M. (2008). 433 Eros lineaments: Global mapping and analysis. *Icarus*, *193*, 39–52.

Buczkowski, D. L., Schmidt, B. E., Williams, D. A., Mest, S. C., Scully, J. E. C., Ermakov, A. I., … Russell, C. T. (2016). The geomorphology of Ceres. *Science*, *353*(6,303), 1004.

Buczkowski, D. L., Sizemore, H. G., Jozwiak, L. M., Schenk, P. M., Scully, J. E. C., von der Gathen, I., … Russell, C. T. (2017). Floor-fractured craters on Ceres: Implications for internal composition and processes, *Lunar and Planetary Science Conference*, *48*, 2117.

Buczkowski, D. L., Wyrick, D. Y., Lyer, L. A., Kahn, E. G., Scully, J. E. C., Nathus, A., … Russell, C. T. (2012). Large-scale troughs on Vesta: A signature of planetary tectonics. *Geophysical Research Letters*, *39*, L18205. https://doi.org/10.1029/2012GL052959

Castillo-Rogez, J. C., & McCord, T. B. (2010). Ceres' evolution and present state constrained by shape data. *Icarus*, *205*, 443–459.

Castillo-Rogez, J. C., Bowling, T., Fu, R. R. CR., McSween, H. Y., Raymond, C. A., Rambaux, N., … Russel, C. T. (2016). Loss of Ceres' icy shell from impacts: Assessment and implications, *Lunar and Planetary Science Conference*, *47*, 3012.

De Sanctis, M. C., Ammannito, E., Raponi, A., Marchi, S., McCord, T. B., McSween, H. Y., … Russell, C. T. (2015). Ammoniated phyllosilicates with a likely outer solar system origin on (1) Ceres. *Nature*, *528*, 241–244.

Drummond, J. D., Carry, B., Merline, W. J., Dumas, C., Hammel, H., Erard, S., … Chapman, C. R. (2014). Dwarf planet Ceres: Ellipsoid dimensions and rotational pole from Keck and VLT adaptive optics images. *Icarus*, *236*, 28–37.

Ermakov, A. I., Park, R. S., Zuber, M. T., Smith, D. E., Fu, R. R., Sori, M. M., Raymond, C. A., … Russell, C. T. (2017). Regional analysis of Ceres' gravity anomalies, *Lunar and Planetary Science Conference*, *48*, 1374.

Ernst, R. E., & Buchan, K. L. (2001). *The use of mafic dike swarms in identifying and locating mantle plumes. Geological Society of America Special Paper*, 352.

Ferrill, D. A., Wyrick, D. Y., & Smart, K. J. (2011). Coseismic, dilational-fault and extension-fracture related pit chain formation in Iceland: Analog for pit chains on Mars. *Lithosphere*, *3*, 133–142.

Fu, R. R., Ermakov, A. I., Marchi, S., Castillo-Rogez, J. C., Raymond, C. A., Hager, B. H., … Russell, C. (2017). The interior structure of Ceres as revealed by surface topography. *Earth Planetary Science Letters*, *476*, 153–164.

Gioia, G., Chakraborty, P., Marshak, S., & Kieffer, S. W. (2007). Unified model of tectonics and heat transport in a frigid Enceladus. *Proceedings of the National Academy of Science*, *104*, 13,578–13,581.

Hiesinger, H., Marchi, S., Schmedemann, N., Schenk, P., Pasckert, J. H., Neesemann, A., … Raymond, C. A. (2016). Cratering on Ceres: Implications for its crust and evolution. *Science*, *353*, aaf4759-1-8.

King, S. D., Bland, M. T., Fu, R., Park, R., Castillo-Rogez, J., Raymond, C. A., Russel, C. T. (2016). 3D spherical convection modeling of the interior of Ceres, *Lunar and Planetary Science Conference*, *47*, 1699.

Lange, M. A., & Ahrens, T. J. (1983). The dynamic tensile strength of ice and ice-silicate mixtures. *Journal of Geophysical Research*, *88*, 1197–1208. https://doi.org/10.1029/JB088iB02p01197

Li, J.-Y., McFadden, L. A., Parker, J. W., Young, E. F., Alan Stern, S., Thomas, P. C., … Sykese, M. V. (2006). Photometric analysis of 1 Ceres and surface mapping from HST observations. *Icarus*, *182*, 143–160.

Longobardo, A., Palomba, E., De Sanctis, M. C., Zinzi, A., Scully, J. E. C., Capaccioni, F., … Russell, C. T. (2015). Mineralogical and spectral analysis of Vesta's Gegania and Lucaria quadrangles and comparative analysis of their key features. *Icarus*, *259*, 72–90.

Manga, M., & Wang, C.-Y. (2007). Pressurized oceans and the eruption of liquid water on Europa and Enceladus. *Geophysical Research Letters*, *34*, L07202. https://doi.org/10.1029/2007GL029297

Marchi, S., Ermakov, A. I., Raymond, C. A., Fu, R. R., O'Brien, D. P., Bland, M. T., … Russell, C. T. (2016). The missing large impact craters on Ceres. *Nature Communications*, *7*(12257), 1–9.

Martin, E. S., Kattenhorn, S. A., Collins, G. C., Michaud, R. L., Pappalardo, R. T., & Wyrick, D. Y. (2017). Pit chains on Enceladus signal the recent tectonic dissection of the ancient cratered terrains. *Icarus*, *294*, 209–217.

McCord, T. B., & Sotin, C. (2005). Ceres: Evolution and current state. *Journal of Geophysical Research*, *110*, E050091. https://doi.org/10.1029/2004JE002244

Mitri, G., Park, R. S., Castillo-Rogez, J., Raymond, C., & Russell, C. T. (2017). Crustal structure and internal differentiation of the dwarf planet Ceres. *European Geosciences Union*, *19*, 12,461.

Neveu, M., & Desch, S. J. (2015). Geochemistry, thermal evolution, and cryovolcanism on Ceres with a muddy ice mantle. *Geophysical Research Letters*, *42*, 10,197–10,206. https://doi.org/10.1002/2015GL066375

Nimmo, F. (2004). Stress generated in cooling viscoelastic shells: Application to Europa. *Journal of Geophysical Research*, *109*, E12001. https://doi.org/10.1029/2004JE002347

O'Brien, D. P., Travis, B. J., Feldman, W. C., Sykes, M. V., Schenk, P. M., Marchi, S., Russell, C. T. (2015). The potential for volcanism on Ceres due to crustal thickening and pressurization of a subsurface ocean, *Lunar and Planetary Science Conference*, *46*, 2831.

Park, R. S., Konopliv, A. S., Bills, B. G., Rambaux, N., Castillo-Rogez, J. C., Raymond, C. A., … Preusker, F. (2016). A partially differentiated interior for (1) Ceres deduced from its gravity field and shape. *Nature*, *537*, 515–517.

Petrovic, J. J. (2003). Review mechanical properties of ice and snow. *Journal of Materials Science*, *38*, 1–6.

Preusker, F., Scholten, F., Matz, K.-D., Elgner, S., Jaumann, R., Roatsch, T., … Russell, C. T. (2016). Dawn at Ceres—Shape model and rotational state, *Lunar and Planetary Science Conference*, *47*, 1954.

Roatsch, T., Kersten, E., Matz, K.-D., Preusker, F., Scholten, F., Jaumann, R., … Russell, C. T. (2016). High-resolution Ceres high altitude mapping orbit atlas derived from Dawn framing camera images. *Planetary and Space Science*, *129*, 103–107.

Russell, C. T., Raymond, C. A., Ammannito, E., Buczkowski, D. L., De Sanctis, M. C., Hiesinger, H., … Yamashita, N. (2016). Dawn arrives at Ceres: Exploration of a small, volatile-rich world. *Science*, *353*, 1008–1010.

Schmedemann, N., Neesemann, A., Schulzeck, F., Krohn, K., von der Gathen, I., Otto, K. A., … Russell, C. T. (2017). The distribution of impact ejecta on Ceres, *Lunar and Planetary Science Conference*, *48*, 1233.

Scully, J. E. C., Yin, A., Russell, C. T., Buczkowski, D. L., Williams, D. A., Blewett, D. T., … Raymond, C. A. (2014). Geomorphology and structural geology of Saturnalia Fossae and adjacent structures in the northern hemisphere of Vesta. *Icarus*, *244*, 23–40.

Thomas, P. C., Parker, J. W., McFadden, L. A., Russell, C. T., Stern, S. A., Sykes, M. V., & Young, E. F. (2005). Differentiation of the asteroid Ceres as revealed by its shape. *Nature*, *437*, 224–226.

Travis, B. J. & Feldman, W. C. (2016). Ceres model suggests large scale topography may reflect early time internal convection, *Lunar and Planetary Science Conference*, *47*, 2762.

Wyrick, D., Ferrill, D. A., Morris, A. P., Colton, S. L., & Sims, D. W. (2004). Distribution, morphology, and origins of Martian pit crater chains. *Journal of Geophysical Research*, *109*, E06005. https://doi.org/10.1029/2004JE002240

Yin, A., Zuzaa, A. V., & Pappalardo, R. T. (2016). Mechanics of evenly spaced strike-slip faults and its implications for the formation of tiger-stripe fractures on Saturn's moon Enceladus. *Icarus*, *266*, 204–216.

Zolotov, M. Y. (2009). On the composition and differentiation of Ceres. *Icarus*, *204*, 183–193.